SANDIA REPORT
SAND2023-09639
Printed September 2023

Sandia National Laboratories

M^+(M=Ca, Ba) Cations Bound to Molecular Cavities:

A New Strategy for Incorporating Molecular Quantum States into Quantum Information

Timothy S. Zwier

Prepared by
Sandia National Laboratories
Albuquerque, New Mexico
87185 and Livermore,
California 94550

Issued by Sandia National Laboratories, operated for the United States Department of Energy by National Technology & Engineering Solutions of Sandia, LLC.

Available to DOE and DOE contractors from
U.S. Department of Energy
Office of Scientific and Technical Information
P.O. Box 62
Oak Ridge, TN 37831

Telephone: (865) 576-8401
Facsimile: (865) 576-5728
E-Mail: reports@osti.gov
Online ordering: http://www.osti.gov/scitech

Available to the public from
U.S. Department of Commerce
National Technical Information Service
5301 Shawnee Rd
Alexandria, VA 22312

Telephone: (800) 553-6847
Facsimile: (703) 605-6900
E-Mail: orders@ntis.gov
Online order: https://classic.ntis.gov/help/order-methods/

ABSTRACT

This project pursued a novel strategy for incorporating multiple qubits per ion into ion-trap based quantum computing (ITQC) involving Ca^+ and Ba^+. By forming molecular complexes of these cations with molecular-scale cages, we hypothesized that molecular energy levels could be incorporated into quantum computing while retaining key properties of the atomic ions intact. We experimented with a variety of molecular cages and found that Na^+, K^+, Rb^+, Ca^{2+}, Sr^{2+}, and Ba^{2+} could be captured and brought into the gas phase efficiently by imbedding them inside [2.2.2]-benzocryptand. IR and UV spectra of these cage complexes are sensitive to the size and charge state of the ion, reporting on the structures and binding properties of the cage complexes. UV photofragmentation of the Ba^{2+}-$Acetate^{-1}$-BzCrypt complex produces Ba^+-BzCrypt, the complex targeted for exploration in the original hypothesis. Follow-on funding is needed to pursue the spectroscopy of this complex as a target for ITQC.

ACKNOWLEDGEMENTS

The authors would like to acknowledge the contributions of Edwin L. Sibert III (UW-Madison), an unfunded external collaborator, who developed and refined a local mode anharmonic model that was important to our fitting of the infrared spectra that we recorded in the alkyl CH stretch region.

CONTENTS

LIST OF FIGURES

This page left blank

EXECUTIVE SUMMARY

This project pursued a novel strategy for incorporating multiple qubits per ion into ion-trap based quantum computing (ITQC). Our hypothesis was that by imbedding the same atomic ions (e.g., Ca^{+}, Ba^{+}) used in current quantum computers inside molecular cavities (MC), molecular vibrational and rotational energy levels would naturally be incorporated into the atomic ion states through their perturbations on the atomic ion. We hypothesized that with the right choice of molecular cavity, the key properties of the atomic ions important for ion-trap quantum computing would remain intact, enabling usage of the same laser technology.

Our experimental approach involved forming Ca^{2+} or Ba^{2+}-molecular cavity complexes in solution and bringing them into the gas phase via electrospray ionization. We used a multi-stage mass spectrometer outfitted with a cryo-cooled octupole ion trap in which we would cool the ions and record their electronic and vibrational spectra via laser photofragmentation. After mass selection and cryo-cooling the ions to 5K in an octupole trap, we interrogated the ions in the infrared and the ultraviolet. These spectra report in exquisite detail on the way the molecular cavity affects the ion and vice versa. Our ultimate goal has been to study the electronic excited states of the Ca^{+}- and Ba^{+}-molecular cavity complexes to compare with the corresponding states in the isolated +1 cations, mapping the molecular states that could play a role in increasing the number of qubits per ion.

After experimenting with several different molecular cavities, we chose [2.2.2]-benzocryptand (BzCrypt) to explore in depth, as it provided a three-dimensional cavity in which the cations fit snuggly. We recorded ultraviolet and infrared spectra of a series of six M^{n+}-BzCrypt cages, where M^{n+}=Na^{+}, K^{+}, Rb^{+}, Ca^{2+}, Sr^{2+}, and Ba^{2+}. Our studies provide unique insight to the way in which a molecular cage reports on its ionic contents via the changes induced by the presence of the ion on the infrared and ultraviolet spectra of the molecular cage. One of the high-risk challenges of the project was to devise a scheme for forming the Ba^{+1} or Ca^{+1}-molecular cavity complexes efficiently, when their natural charge state is +2. After considering charge reduction via ion-ion reactions, we devised a modified strategy that forms an ion-pair complex between the +2 ion inside the cage and an anion with -1 charge (e.g., Ba^{2+}-$Acetate^{-1}$-BzCrypt). Following either collisional excitation or UV excitation, electron transfer from the acetate anion to Ba^{2+} followed by loss of the neutral acetate radical led to formation of Ba^{+1}-BzCrypt, albeit at modest levels. Follow-on funding is needed to pursue the optical spectroscopy of this complex as a potential candidate for ion-trap quantum computing.

ACRONYMS AND TERMS

Acronym/Term	Definition
ITQC	Ion Trap Quantum Computing
MC	Molecular Cavity
[n]-CPP	n-cycloparaphenylene
BzCrypt	[2.2.2]-benzocryptand
OAc	Acetate anion
•OAc	Neutral acetoxy radical

1. INTRODUCTION

A defining starting point for current ion trap quantum computing (ITQC) is that each atomic ion serves as a single qubit.[1] Atomic ions with single valence-shell electrons (e.g., Ca^+, Yb^+, Ba^+) have simple energy level structures (see Figure 1a) with electronic transitions for cooling and qubit state preparation and read-out at wavelengths where compact, high-resolution lasers operate effectively. In Ca^+, the $4^2S_{1/2}$-$4^2P_{1/2}$ transition at 397 nm is used to laser cool the Ca^+ inside the ion trap into a linear array with spacing determined by the balance between inter-ion Coulomb repulsion and the electrostatic trapping potential. The quadrupole-allowed $4S_{1/2}$-$3D_{5/2}$ transition at 729 nm serves as the atomic qubit, with a spontaneous emission lifetime of ~1 sec. Individual qubits are entangled by state-dependent coupling to the vibrational motions of the ions in the trap, while read-out of the states of the individual qubits occurs via fluorescence.[1, 2]

Molecular ions offer a tantalizing prospect for moving well beyond the one qubit per ion limit.[3] Imbued with resolvable internal degrees of freedom due to the reduction in electronic symmetry, molecular vibration and rotation, one can imagine a long-term future in which quantum computers carry out their processes via coherences between this array of internal states within each molecular ion. A common-sense strategy for moving in this direction is in chemically-bound diatomic ions, with their simple vibration-rotation energy level structure.[4-7] However, the chemical bond drastically alters the electronic structure of the individual atoms, necessitating reconsideration of all aspects of their optical control. Nevertheless, it is still possible to sympathetically cool the molecular ions into a Ca^+ coulomb crystal and even to study their spectroscopy through the perturbations associated with electronic excitation of the diatomic ion affecting a Ca^+ quantum logic operation, a clever new kind of 'action' spectroscopy with Ca^+ atomic ion read-out.[4-7]

In this LDRD grant, we pursued a novel strategy for incorporating molecular degrees of freedom into ion trap quantum computing and sensing; namely, to bind the same atomic ions used for quantum computing (e.g., Ca^+) inside neutral molecules shaped to serve as a molecular cavity (MC) for the ion. Our hypothesis was that the ion-MC complex will have molecular energy levels that are exquisitely sensitive to the size and shape of the MC binding partner, while retaining the essential

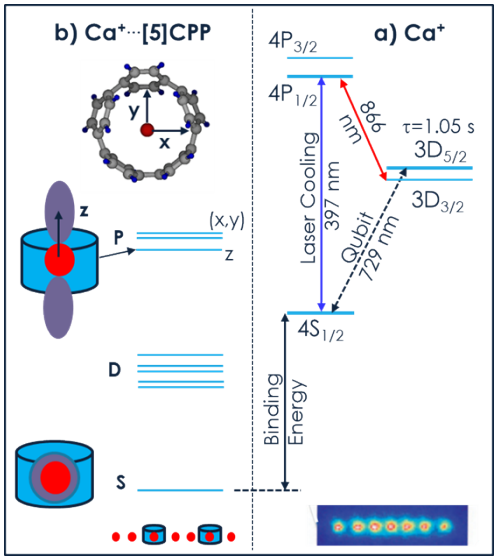

Figure 1. Electronic energy level diagram for a) atomic Ca^+ and b) the Ca^+-[5]CPP complex.

exceptional electronic properties of the atomic cations that make them the ions of choice for quantum computing. We postulated that the small size of the molecular cavity will lead to resolvable, electronic-state dependent vibrational and rotational 'fine structure' that will appear in the electronic spectrum of the Ca^+-MC complex and could be used to encode additional quantum information if coherently prepared.

Backed by promising computational work by our SUPN collaborators, we hypothesized that the [n]-cycloparaphenylenes, labeled [n]-CPP, were good first candidates.[8] These fascinating and beautiful macrocycles are made up of 'n' aromatic rings concatenated together to form a belt inside which a cation could fit, as shown for [5]-CPP in Figure 1(b). They have been synthesized with sizes ranging from n=5-20, with interior radii stretching from 0.6-2.0 nm. The computational predictions mapped out the potential energy surfaces for motion of Ca^+ inside these [n]CPP cages as a function of size 'n', predicting that the global minimum is at the center of the cage through n=6, but prefers an off-center position for n≥7. While these macrocycles did not turn out to be optimal for our mass-spectrometry based studies, they nevertheless serve as an apt illustration of the effects of a molecular cavity on the electronic states of Ca^+. In Figure 1, a schematic electronic energy level diagram for Ca^+-[5]-CPP is shown, offset from Ca^+ by its calculated binding energy (220 kJ/mol).

The ^2S-^2P transition at 397 nm in Ca^+ (Figure 1a) promotes the single 4s electron into a 4p orbital, which is triply degenerate. However, the presence of a non-spherical molecular cavity around the ion will split this degeneracy and the degeneracy of the five 3d orbitals in the 3D excited states. Thus, the **electronic state splitting and patterns** reflect the response of the Ca^+ valence electron to the molecular cavity. We thus anticipate the presence of several excited electronic states, with transitions from the ground state near the wavelengths of the Ca^+ atomic transitions used for ITQC.

Furthermore, each electronic state will support sets of vibrational levels, whose Franck-Condon intensities in absorption reflect the changes in geometry of Ca^+-MC in the excited state relative to the ground state. To the degree that electronic excitation is localized on the Ca^+, we anticipated largest Franck-Condon activity involving the **vibrations of the Ca^+ in the molecular cavity**, directly reporting on the shape of the molecular cavity potential in which it moves.

While the primary application of our studies was towards quantum information, the studies of ions confined inside molecular cavities has many other important applications, including selective extraction of ions from the environment,[9, 10] capture of ions in unusual charge states where electron transfer to and from other reactants could be controlled,[11] or the study of catalytically active ions,[12, 13] where binding to the cavity could be used to fine-tune its catalytic activity.

In what follows, we describe our efforts to find the best molecular cavities in which to sequester alkaline earth cations, introduce the cryptands as our eventual molecular cavity of choice, and describe a wide-ranging set of studies of the ultraviolet and infrared spectra of ions inside [2.2.2]-benzocryptand, labeled as BzCrypt, with structure shown to the right. By incorporating a UV chromophore into the 'walls' of the cryptand cavity, we are afforded a spectroscopic handle of the cryptand cavity's response to the ion inside it. We shall also describe some preliminary success with a new strategy for charge reduction of the +2-charged alkaline earth cations to the desired +1 charge state. This involves formation of an M^{2+}-X^{-1}-BzCrypt ion pair complex followed by collisional or laser excitation to initiate electron transfer from X^- to M^{2+}, leading to loss of neutral X from the complex, thereby forming M^+-BzCrypt.

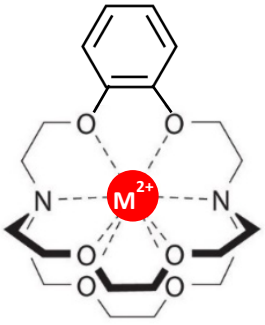

2. EXPERIMENTAL AND COMPUTATIONAL METHODS

2.1. Experimental

The experimental work was carried out in an apparatus shown in schematic form in Figure 2.[14] Nano-electrospray ionization (n-ESI) was used to bring the M^{n+}-BzCrypt complexes into the gas phase. The BzCrypt sample was available commercially. It was dissolved in a 50:50 H_2O/CH_3OH solution at 200 μM concentration. The salts used as the source of the M^{n+} cations were dissolved separately and added to the mixture in some excess, ranging from 1:1 to 8:1 ratio of M^{n+}:BzCrypt. This produced a clean source of the M^{n+}-BzCrypt complexes. In the Ba^{2+}-BzCrypt complexes, we used barium acetate salt, $Ba(OAc)_2$, where OAc = $CH_3CO_2^-$. Depending on electrospray and tuning conditions, we could find conditions in which $[Ba\text{-}OAc\text{-}BzCrypt]^+$ complexes at m/z 621 were also produced, a novel ion-pair complex whose spectroscopy we also pursued.

Ions from the electrospray source were stored in a linear quadrupole ion trap (Q2) before mass selection of the parent ion of interest using rf/dc (apex) isolation.[15] This process also serves as an annealing step, as the parent ion is placed near the stability limit where it experiences annealing collisions with the trapping gas (helium). The mass selected ions are transported to an octupole ion trap cooled by a closed cycle refrigerator to 5 K. Helium pulsed into the trap serves as trapping gas and provides a mechanism for cooling the internal degrees of freedom of the ions.

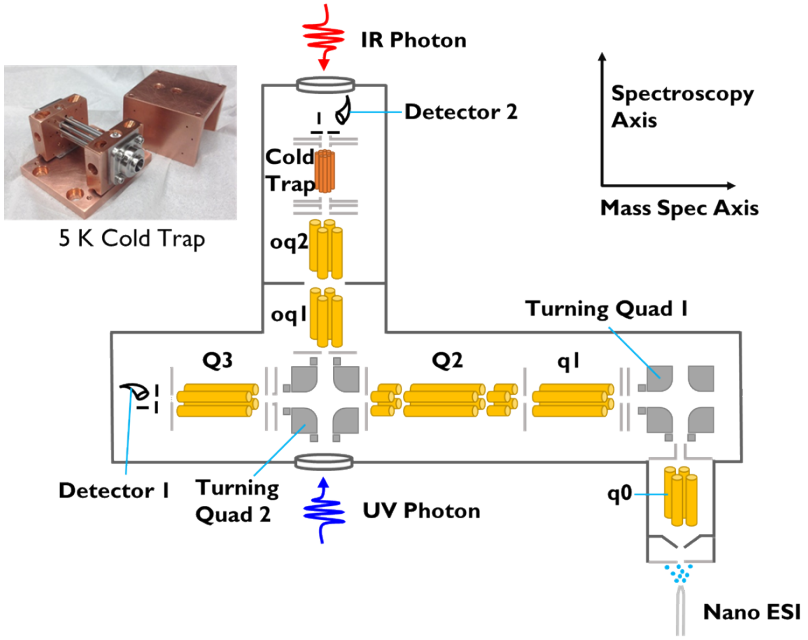

Figure 2. Schematic diagram of the multi-stage mass spectrometer used to record IR and UV spectra of cryo-cooled ions.

UV photofragment spectra (Figure 3, blue trace upper right) were recorded using the doubled output of a Nd:YAG pumped dye laser (Coumarin 540A) covering the 35,400 – 37,500 cm^{-1} region operating at 10 Hz. UV excitation led to photo-fragmentation of a few percent of the parent ions in the octupole trap. After UV excitation, parent and fragment ions were released from the trap to an analysis linear quadrupole ion trap Q3 that operates in one of two modes. When recording a UV spectrum, resonant ejection is used to selectively remove parent ions from the trap ('parent knock-out') prior to collection of all remaining UV photofragment ions independent of their mass.

Alternatively, the mass spectrum of the photofragment ions can be recorded at a fixed UV wavelength. In order to record UV or IR spectra at the 10 Hz repetition rate of the Nd:YAG lasers, the ions were shuttled from ion source through mass selection, into the cold trap, undergo fragmentation, and are brought back to Q3 for mass analysis on the 100 ms timescale.

A Nd:YAG-pumped optical parametric converter (OPC) was used as IR laser source, also operating at 10 Hz. IR pulse energies of ≤10 mJ/pulse were used, tunable from 2000-4000 cm^{-1} at a resolution of $\Delta\tilde{\nu} \approx 3$ cm^{-1}. When extension of the IR spectra into the mid-IR region (1000-2000 cm^{-1}) was required, an angle-tuned $AgGaSe_2$ crystal was inserted after the final stage of the OPC, using difference frequency mixing to produce the mid-IR wavelengths of interest. This process leads to tunable IR operating in the 1000-2000 cm^{-1} region, with about 5-10 times less power (1-2 mJ/pulse) than in the 2400-3800 cm^{-1} region.

IR-UV double resonance is used to record ground state infrared spectra via one of two methods. IR-UV ion dip spectra (Figure 3) are recorded by fixing the UV wavelength on a single vibronic transition of the parent ion so that the photofragment ion signal is due to the single conformation responsible for this absorption. The IR output was spatially overlapped with the UV laser in the cold ion trap, but temporally precedes the UV by ~100 ns. When the IR wavelength is resonant with a vibrational transition of the monitored ion conformation, absorption removes population from the vibrational zero-point level, resulting in a dip in the cold UV photofragment signal.

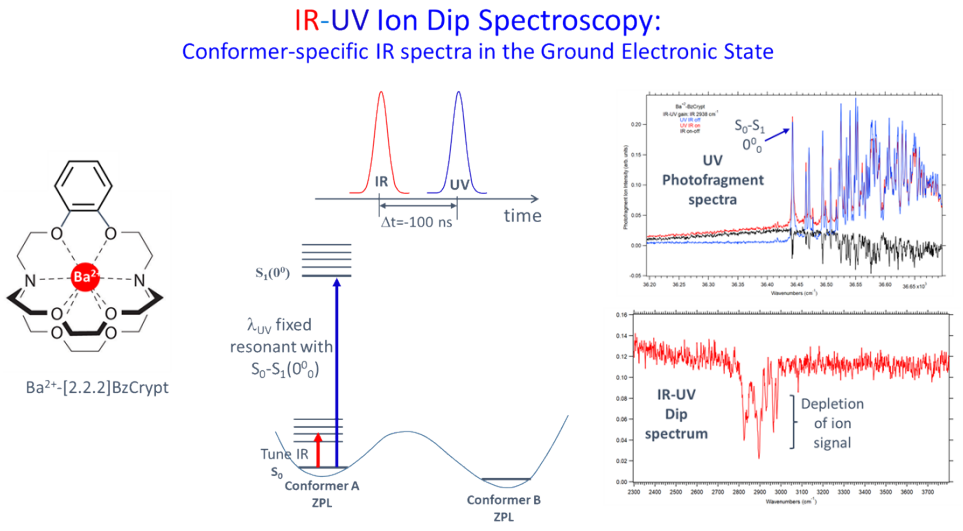

Figure 3. Schematic diagram of IR-UV Ion Dip Spectroscopy, using Ba^{2+}-BzCrypt as example. The UV photofragment spectrum and IR-UV dip spectrum are shown in the upper and lower right.

By contrast, in IR gain spectroscopy (Figure 4), the UV laser is fixed off-resonance from any UV transitions of the cold ion (wavelength position marked with the arrow in the upper right UV spectrum). Since IR excited molecules possess a broadened UV absorption spectrum (rising baseline in red in the upper right), this broadened absorption can partially cancel the depletion signal on-resonance (dips in black trace) or can produce a gain signal when the UV is off-resonance. At the off-resonant UV wavelength, an IR gain spectrum is recorded by tuning the IR wavelength. These spectra are against zero background (ideally) but are no longer conformation-specific because any conformation that absorbs the IR will create a broadened gain signal in the UV. Importantly, when the IR gain and dip spectra match, it is a strong indication that only one conformer of the parent ion is present in the cryocooled ion trap.

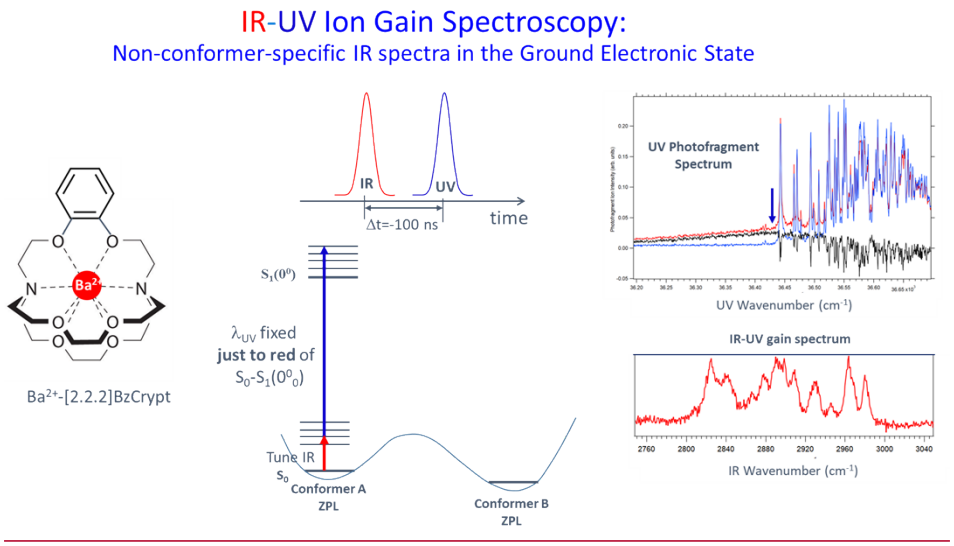

Figure 4. Schematic diagram of IR-UV Ion Gain Spectroscopy, using Ba^{2+}-BzCrypt as example. The UV photofragment spectrum and IR-UV gain spectrum are shown in the upper and lower right.

In the studies described here, overview IR spectra in the 2400-3800 cm^{-1} region were supplemented with shorter scans in the alkyl CH stretch region (2800-3000 cm^{-1}). It is this latter region that is diagnostic of the conformation of the benzocryptand cage and how it changes with the size and charge of the M^{n+} ion. Our studies included benzocryptand complexes with the singly charged alkali metal cations Na^+, K^+, and Rb^+ and doubly charged alkaline earth cations Ca^{2+}, Sr^{2+}, and Ba^{2+}.

2.2. Conformational Searches

The experimental IR spectra were assigned to specific conformations of the benzocryptand molecular cavity by comparing the single-conformation IR spectra from experiment to the IR spectra predicted by calculations, consisting of vibrational frequencies and IR intensities of individual conformational minima. As a result, the first step is to map out the conformational minima for the M^{n+}-BzCrypt complexes.

We carried out conformational searches for the M^{n+}-BzCrypt complexes based on molecular dynamics (MD) simulations using TINKER software[16] with the AMOEBA force field[17]. The automated parameterizing program POLTYPE2 was used to generate AMOEBA parameters for BzCrypt and the ion parameters were taken from amoebabio18.prm. Starting structures for the M^{n+}-BzCrypt MD simulations were provided by X-ray crystal structures for [2.2.2]benzocryptand with the ions placed at the midpoint between the two capping nitrogens in the cryptand cage. We carried out simulations of the complexes at high temperature (1000K) for 50 ns[18] to search conformational space, with one structure frame saved every 5 ps. Each frame was then minimized using TINKER with the AMOEBA force field.

For each M^{n+}-BzCrypt complex, we grouped the ensemble of optimized structures into 20 closely similar 'clusters' of structures using the K-means clustering algorithm of Lightweight Object-Oriented Structure-analysis (LOOS).[19] Representative frames from the clusters were taken as starting points for quantum mechanical (QM) structure optimization using Gaussian16 software.[20] We took the most similar frames instead of the generated cluster structures to ensure that the structures used for DFT optimization were ones sampled by the MD simulation.[21, 22] The DFT calculations employed the TPSSTPSS functional with mixed atomic basis sets that used cc-pVTZ for H

(hydrogen), aug-cc-pVTZ for C (carbon), O (oxygen), and N (nitrogen), the MWB64 pseudopotential with associated basis set for elements low in the periodic table (e.g., Ba^{2+}), and a 6-311++G(2d,2p) basis set for the others (e.g., K^+). These functionals and basis sets were chosen based on previous studies of similar ions.[23, 24] The energies of these optimized structures were then compared to determine the lowest energy structure from each cluster. Based on this energy ordering, other members of the lowest energy structures from the groups were taken as starting structures for structure optimization. As a final check for completeness, random searches were performed through dihedral angle space for each of the three strands looking for structures that satisfied a reasonable N-N distances for ion contact and had reasonable O-C-C-O dihedrals to get metal ion bonding. The lowest energy structures from this search were compared to those from the MD clusters to ensure completeness. In a few cases, the random searches identified a slightly lower energy structure than the ones chosen from the representative cluster structures. We combined these two searches to form a set of structures on which to carry out vibrational analysis. Binding energies for the assigned structures were computed at the same levels of theory, including corrections for both zero-point energy and basis set superposition error (BSSE).[16]

2.3. Modeling of the alkyl CH stretch region

The benzocryptand cage has a total of 16 CH_2 groups spaced along the three interconnecting ether bridges (Figure 3), with each CH_2 contributing two CH stretch transitions to the IR spectrum in the alkyl CH stretch region (2800-3000 cm^{-1}), leading to structures but highly congested spectra. Furthermore, pervasive and strong Fermi resonances of the CH stretch vibrations with the overtones (v=2 states) of the CH bends, produces spectra that are not possible to fit without explicitly modeling these Fermi resonances. Ned Sibert (UW-Madison) has developed a local mode, anharmonic model of the CH stretch region that takes explicit account of these complexities. In the context of this project, he extended the model to the strong-binding circumstances present in the M^{n+}-BzCrypt complexes, working as an unfunded external collaborator. The details of this model are beyond the scope of this report, but are provided in our recent publication on K^+/Ba^{2+}-BzCrypt complexes.[25] With this model, he was able to obtain quantitative fits of the alkyl CH stretch spectra, leading to firm assignments for most of the complexes studied as a part of this work.

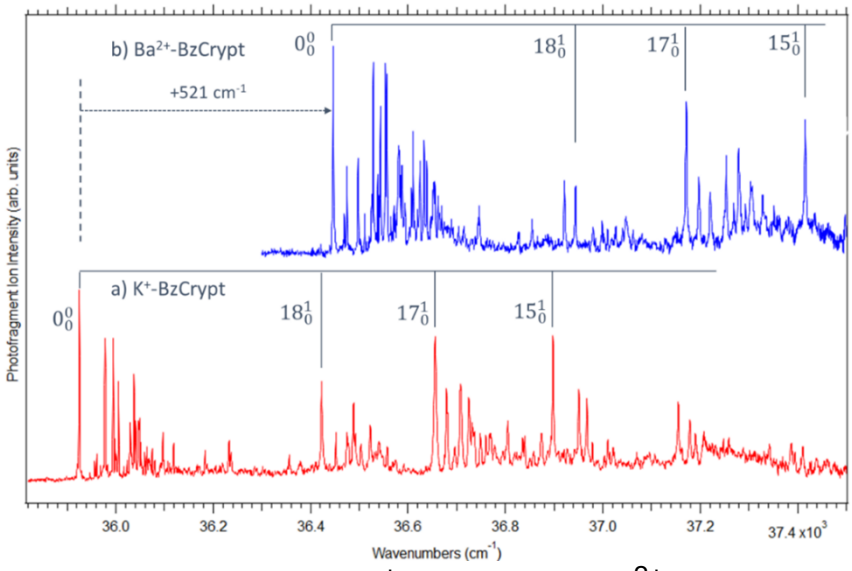

Figure 5. UV photofragment spectra of (a) K^+-BzCrypt and (b) Ba^{2+}-BzCrypt complexes in the region of their S_0-S_1 transitions. Tentative assignments are given for the vibronic transitions using the notation in Tuttle et al.[26] appropriate for ground state vibrations in ortho-disubstituted benzenes.

3. RESULTS AND ANALYSIS

3.1. The K^+/Ba^{2+}-BzCrypt Pair[25]

Figure 5 shows overview UV photofragment spectra of K^+-BzCrypt and Ba^{2+}-BzCrypt complexes in the region where the phenyl ring in the structure is known to absorb. The S_0-S_1 origin of K^+-BzCrypt is at 35,925 cm^{-1} (278.36 nm), while that for Ba^{2+}-BzCrypt is shifted 521 cm^{-1} further to the blue, appearing at 36,446 cm^{-1} (274.38 nm). Both UV photofragment spectra have a rather dense set of low-frequency vibronic activity and vibronic structure at higher frequency that reflect localized structural changes in the phenyl ring upon $\pi\pi^*$ excitation, involving in-plane ring deformation (ν_{18}, ν_{15}) and ring breathing (ν_{17}) motions. The shift in the electronic origin is a first way in which the benzocryptand cage responds differently to the ion imbedded inside it. Since the K^+ and Ba^{2+} are nearly the same size (152/149 pm), the major effect of this blue shift is the difference in charge.

Figure 6(a) shows the alkyl CH stretch spectra of K^+-BzCrypt and Ba^{2+}-BzCrypt. The close correspondence between the IR-UV dip and gain spectra of the K^+-BzCrypt complex indicates that there is a single dominant conformation present in our mass spectrometer, so that only absorptions due to this single conformer contribute to the gain spectrum, which is not conformer specific. The analogous IR-UV dip spectrum of Ba^{2+}-BzCrypt is surprisingly different from that of K^+-BzCrypt, most notably in having the lower-frequency portion of the spectrum shifted to higher wavenumber.

Figure 6(b) displays the calculated alkyl CH stretch spectra from the anharmonic local mode model for structures A and B of K^+-BzCrypt, while the analogous results for Ba^{2+}-BzCrypt are shown in Figure 6(c). In the K^+-BzCrypt complex, structure A provides an excellent fit to the experimental spectrum, significantly better than that of conformer B or any other of the calculated spectra, leading to an unambiguous assignment of the experimental structure to conformer A, shown from two viewpoints in Figure 7a). On the other hand, the calculated spectra for structures A and B in Ba^{2+}-BzCrypt are not as obviously different. While the fit is somewhat better for A than B, the smaller energy difference (168 cm^{-1}) prevents a completely firm assignment.

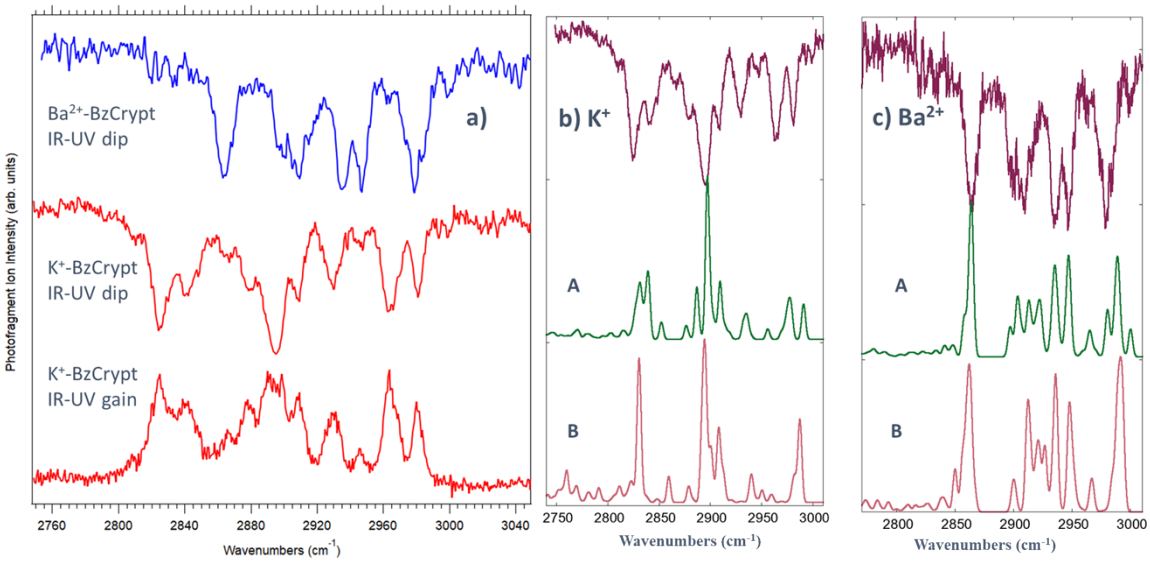

Figure 6. (a) Comparison of the IR-UV gain and dip spectra of K^+-BzCrypt (red) and the corresponding IR-UV dip spectrum of Ba^{2+}-BzCrypt (blue). Experimental IR-UV dip spectra (top) compared to theoretical predictions (middle and lower traces) for conformers A and B of (b) K^+-BzCrypt and (c) Ba^{2+}-BzCrypt cage complexes, whose structures are shown in Figure 7.

The assignment of conformer A of K^+-BzCrypt as the experimentally observed structure and the analogous assignment of Ba^{2+}-BzCrypt to its analogous conformer A is striking, indicating that these similarly sized ions bind to the cage in closely analogous ways. Note that conformer A is the calculated global minimum energy structure in both complexes; that is, the conformations of the benzocryptand cage around the two ions that is lowest in energy. Conformer A is less symmetric than conformer B, most notably, in the phenyl ring bending away from vertical. This subtle structural difference has clear spectral consequences for the alkyl CH stretch region (Figure 7b, c).

One of the strengths of the anharmonic model of the alkyl CH stretch region is that it provides additional understanding regarding which CH stretch modes are responsible for which absorptions in the spectrum. While a detailed analysis is outside the scope of this report, it is worth noting that the lowest frequency portion of the spectrum arises from CH_2 groups adjacent to the capping N atoms of the cage. These transitions are shifted to higher wavenumber in the presence of Ba^{2+} compared to K^+, providing yet another means by which the benzocryptand cage reports on its ionic contents through its IR spectroscopic signatures. The reason for this shift is described in more detail in the published manuscript describing this work.[25]

Finally, we recorded mass spectra of the photofragments of the K^+-BzCrypt and Ba^{2+}-BzCrypt complexes with the UV laser fixed on their corresponding S_0-S_1 electronic origins. The mass spectra for K^+-BzCrypt are shown in the supplementary material for our published manuscript.[25] The main peaks involve loss of C_2H_4 (28 amu) and H_2CO (30 amu) from the complex. These are small fragments of the alkyl ether chains (-CH_2-CH_2- and -CH_2-O-) that make up the cage walls.

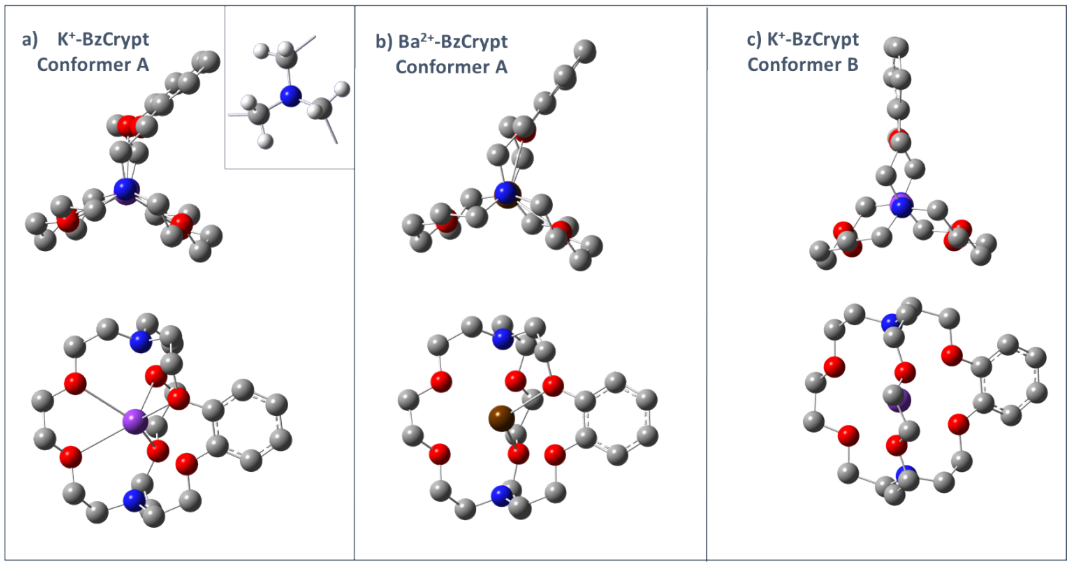

Figure 7. End-on (top) and side (bottom) views of optimized structures for the global minima (conformer A) of (a) K^+-BzCrypt and (b) Ba^{2+}-BzCrypt complexes and (c) the second lowest energy structure of K^+-BzCrypt (conformer B), with hydrogens hidden for clarity.

3.2. Extension to other M^{n+}-BzCrypt Complexes[27]

In order to gain a more complete understanding of the way in which the benzocryptand cage interacts with ions of a greater range of sizes and charge states, we have extended our studies of the structures and spectroscopy of the M^{n+}-BzCrypt complexes to include the alkali metal +1 cations M^+ = Na^+, K^+, Rb^+ and the alkaline earth +2 cations Ca^{2+}, Sr^{2+}, and Ba^{2+}. Overview UV photofragment spectra of the alkali metal series is shown on the left side of Figure 8, while the right side shows the corresponding members of the alkaline earth series. Note, first, that the UV spectra of the Na^+, Rb^+,

and Ca^{2+} complexes were recorded with the UV focused with a 75 cm lens into the cold trap, and thus produced UV spectra that were partially saturated; that is, the spectra appear more congested due to the higher power densities that increase the relative intensities of small peaks in the spectrum relative to large ones. The unsaturated spectra for K^+, Sr^{2+}, and Ba^{2+} used a collimated UV laser beam (<0.5 mJ/pulse) of 5 mm diameter. Focused conditions were required for Na^+ and Ca^{2+}-BzCrypt because their smaller sized ions have larger binding energies to the BzCrypt cavity, making it more difficult to fragment the complexes with a single UV photon.

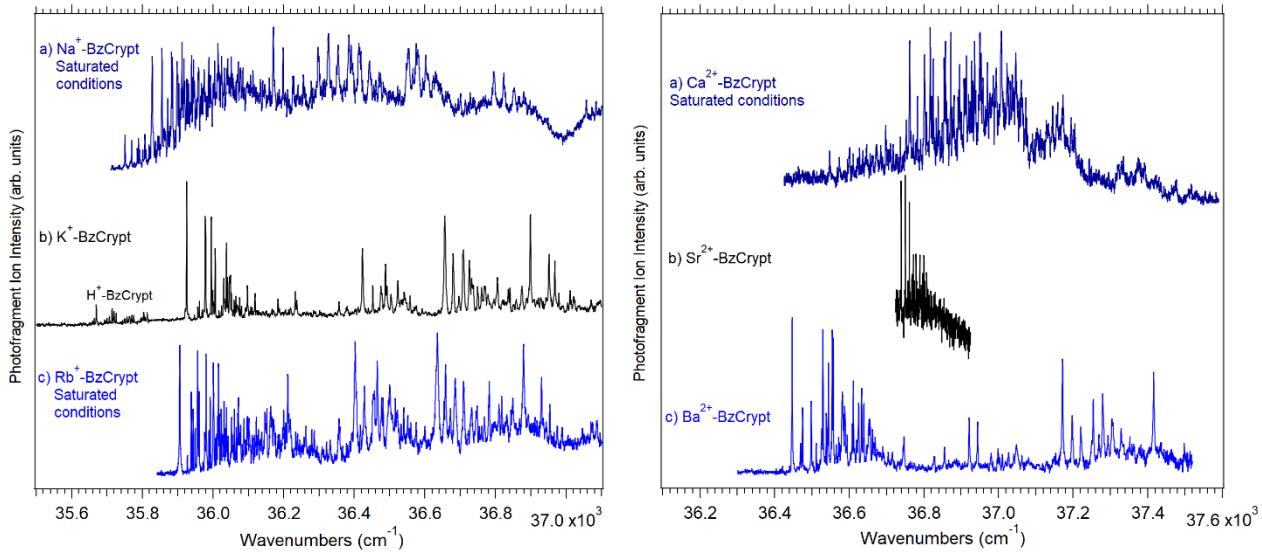

Figure 8. Overview UV photofragment spectra of (left) Na^+-, K^+-, and Rb^+-BzCrypt complexes. (Right): Corresponding spectra of Ca^{2+}-, Sr^{2+}-, and Ba^{2+}-BzCrypt.

The main S_0-S_1 electronic origin transitions for the alkali metal series (left) occur at 35,832 cm^{-1} for Na^+-BzCrypt, 35925 cm^{-1} for K^+-BzCrypt, and 35906 cm^{-1} for Rb^+-BzCrypt, while those for the corresponding alkaline earth cations are at 36765 cm^{-1} for Ca^{2+}-BzCrypt, 36739 cm^{-1} for Sr^{2+}-BzCrypt and 36446 cm^{-1} for Ba^{2+}-BzCrypt. The UV chromophore in BzCrypt is closely equivalent to that in 1,2-dimethoxybenzene (DMB). Based on previous work,[28] the S_0-S_1 origin of isolated DMB neutral molecule is at 35751 cm^{-1}. This serves as a good surrogate for where the electronic origin would be in benzocryptand without any ion inside it. Thus, we use this frequency as a zero for a relative scale that measures the effect of the cations on the $\pi\pi^*$ transition as a function of size and charge state of the ion. Interestingly, the +1 cations show an electronic frequency shift that is smallest for Na^+ (+81 cm but closely similar in K^+-BzCrypt (+174 cm^{-1}) and Rb^+-BzCrypt (+155 cm^{-1}). The M^{2+}-BzCrypt complexes have electronic origins that are shifted much further to the blue, that is, towards larger wavenumbers (shorter wavelengths), than those for M^+-BzCrypt. These shifts are largest for Ca^{2+}-BzCrypt (+1014 cm^{-1}) and Sr^{2+}-BzCrypt (+988 cm^{-1}), but somewhat smaller in Ba^{2+}-BzCrypt (+695 cm^{-1}).

The magnitude of the blue shift of the electronic origin is a measure of how strongly each cation draws electron density away from the two oxygen atoms that are chemically bound to the phenyl ring. The over-all trend is that the +2 cations are significantly more effective at doing so than the +1 charge ions. This trend is illustrated in dramatic fashion when comparing Na^+-BzCrypt to Ca^{2+}-BzCrypt. Notably, Na^+ and Ca^{2+} have very similar ionic radii, but the Ca^{2+}-BzCrypt S_1 origin is almost 1000 cm^{-1} to the blue of Na^+-BzCrypt, with Ca^{2+} having the largest and Na^+ the smallest shift from the unperturbed 1,2-dimethoxybenzene origin.

One might have anticipated that within the +1 or +2 series, similar trends in electronic frequency shifts would be observed, but this is definitely not the case. The electronic frequency shift is exquisitely sensitive to how the ion fits inside the benzocryptand molecular cavity, as it is a localized interaction with the aromatic ring.

The alkyl CH stretch region of the IR provides complementary insight to the structure and binding of the ions to the benzocryptand cavity. The IR-UV dip spectra in Figure 9 show interesting changes along the series. For instance, the spectra of K^+-BzCrypt and Rb^+-BzCrypt and almost identical, while that for Na^+-BzCrypt is distinctly different. The IR spectrum of Sr^{2+} holds much in common with that of Ba^{2+}-BzCrypt in that both have the main transitions shifted to higher wavenumber than the spectra of the alkali metal complexes. As mentioned in the previous section, this shift is ascribed to the CH_2 groups adjacent to the capping nitrogens, indicating that the +2 charge cations have a larger effect on the nitrogen lone pairs than their +1 counterparts.

The Sr^{2+}- and Ba^{2+}-BzCrypt spectra (Figure 9, right) show reproducible differences between them, most notably in the highest frequency transitions that form a doublet in Sr^{2+}-BzCrypt but not in Ba^{2+}-BzCrypt. Note that the Ca^{2+}-BzCrypt IR spectrum is missing from the series. Unfortunately, the photofragment signal of this extremely strongly bound cavity complex was too small to record IR spectra with an acceptable signal-to-noise level, despite significant effort.

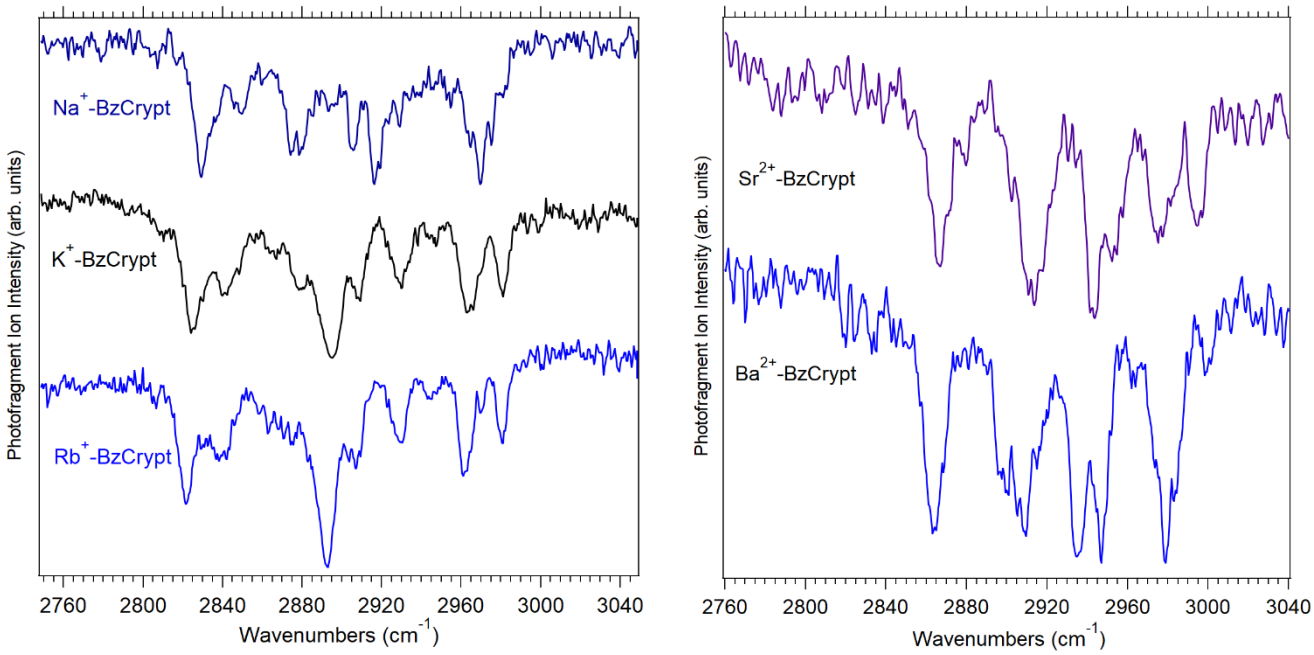

Figure 9. Alkyl CH stretch IR spectra of the set of five M^{n+}-BaCrypt complexes: (left) $Na^+/K^+/Rb^+$-BzCrypt and (right) Sr^{2+}/Ba^{2+}-BzCrypt.

As of the writing of this report, we do not have final assignments for the structures of the entire series. However, we can draw some preliminary conclusions. K^+ and Ba^{2+} are known to be of an ideal size to fit into the [2.2.2]-cryptand cavity, and this is borne out by their structures, in which the cations sit in the center of the cavity (equal distance to the two N atoms), with a largely symmetric structure that is distorted from three-fold symmetry by the bend in the orientation of the aromatic ring (Figure 7). Ions smaller in size than this ideal (e.g., Na^+, Ca^{2+}, Sr^{2+}) must necessarily distort the cavity to maximize total binding energy with the six oxygen atoms and two nitrogen atoms of the

molecular cavity. The final preferred structures in these cases are likely to be a compromise between forming fewer, stronger $M^{n+}\cdots O$ and $M^{n+}\cdots N$ interactions and having more, weaker interactions with the full set of O/N atoms in the cage. When the cation is modestly larger than the K^+/Ba^{2+} pair, with their 152/149 pm 6-coordinate radius, as it is in Rb^+ (166 pm 6-coordinate radius), both the IR and UV spectra are nearly identical to that of K^+, indicating that Rb^+ binds to benzocryptand nearly identically to that in K^+-BzCrypt. We surmise that the cage retains its over-all shape even when slightly over-filled.

3.3. Extension of IR-UV spectra into the mid-IR

While the alkyl CH stretch region of the infrared reports on the cryptand cage with good structural sensitivity, it is also important to extend our infrared spectroscopic probes into the mid-infrared, where other IR absorptions can report on the structure of the complex. In particular, since the primary binding sites of the ion to the cryptand is through the six O atoms, the C-O stretch transitions should report quite directly on this binding geometry and the strength of interaction between the ion and the cage. These IR transitions occur in the mid-IR (1000-1700 cm^{-1}), which required installation of a $AgGaSe_2$ crystal in which difference frequency mixing occurs between the signal and idler beams of our infrared optical parametric oscillator/amplifier (OPO/OPA). This process is not very efficient, making up to 2 mJ/pulse in the mid-IR from a total of 40 mJ/pulse of signal plus idler beams from the IR OPO/OPA. As a result, these spectra require particular care in IR/UV beam overlap and ion signal stability.

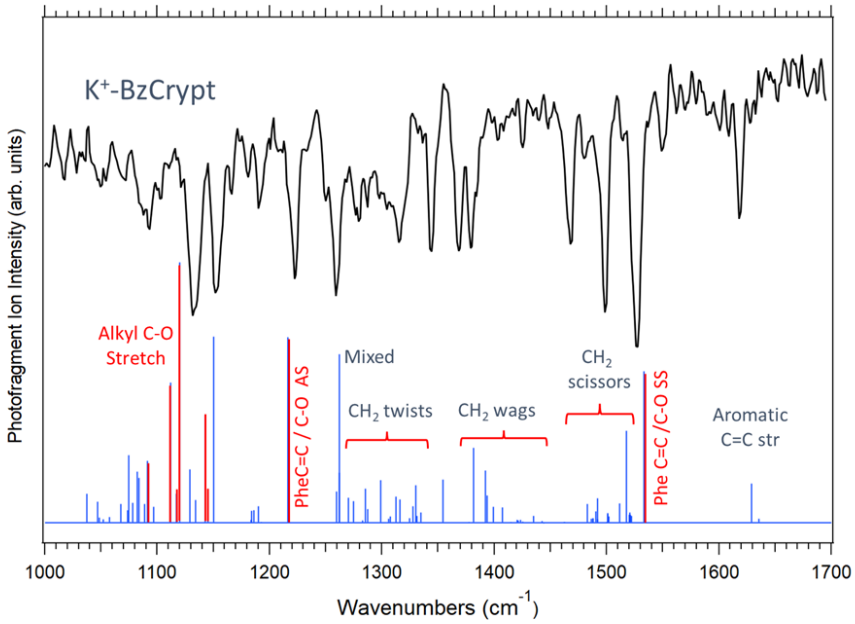

Figure 20. IR-UV dip spectrum of the K^+-BzCrypt complex in the mid-IR region (top) compared with the calculated spectrum of the assigned structure for the complex. The vibrational transitions carrying significant C-O stretch intensity are shown in red.

Figure 10 shows an IR-UV dip spectrum of K^+-BzCrypt over the 1000-1700 cm^{-1} region, compared to a calculated stick spectrum of the vibrational frequencies and IR intensities of the assigned structure of K^+-BzCrypt. The spectrum is congested with transitions due to several different types of vibrations, as indicated in Figure 10. Among them are transitions due to normal modes of vibration that include a lot of C-O stretch motion in them. These are also some of the most intense

IR transitions in this region, probably in part because of the strong interaction of the O-atoms with the K^+. We have color-coded these C-O stretch transitions in red to highlight them. We are still in process of recording mid-IR scans of the full range of M^{n+}-BzCrypt complexes, which we hope will assist with assignments of the structures responsible for them in cases where there is still ambiguity based on the alkyl CH stretch region (Section 3.2).

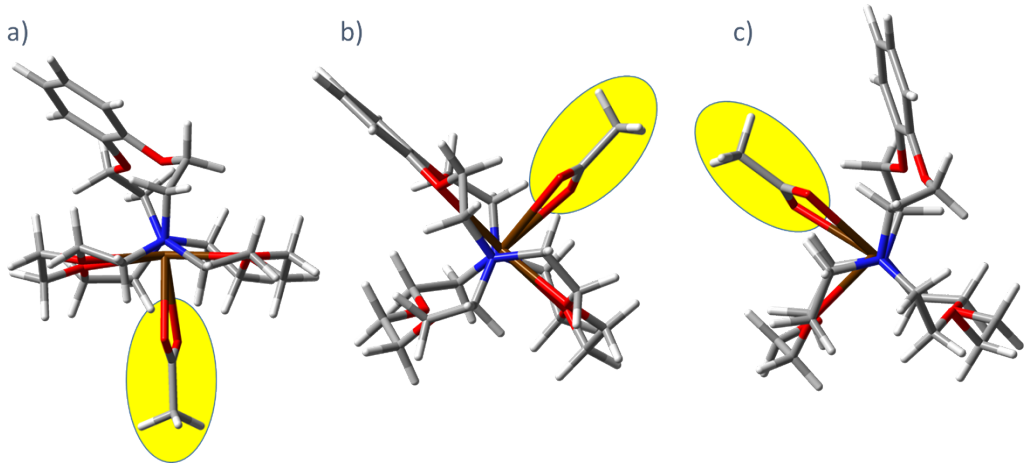

Figure 31. Optimized structures for three contact ion pair [Ba-OAc-BzCrypt]$^+$ geometries in which the acetate anion (yellow shading) binds to Ba^{2+} (maroon) by inserting itself in each of the three crevices between the three walls of the benzocryptand cage. Of the three, the structure shown in a) is lowest in energy ('0' cm^{-1}), while those in b) and c) are 130 cm^{-1} and 380 cm^{-1} higher in energy, respectively.

3.4. Ion Pair-BzCrypt Complexes[29]

3.4.1. The Spectroscopy and Structure of [Ba^{2+}-$Acetate^{1-}$]-BzCrypt

During our studies of Ba^{2+}-BzCrypt, we experimented with both barium chloride and barium acetate as sources of Ba^{2+} ions in the solutions we used to form and electrospray Ba^{2+}-BzCrypt. The acetate anion, $CH_3CO_2^-$ (labeled as OAc) is a common counter-ion used in salts, as it is the basic form of acetic acid, CH_3COOH (HOAc). We noticed that, under gentle electrospray conditions, we would have increasing ion signals at m/z 621, associated with formation of $Ba^{2+}(OAc)^-$-BzCrypt, a complex with over-all charge of +1.

We decided to pursue an investigation of this complex, because it constitutes a Ba^{2+}-OAc^{1-} ion pair in which the Ba^{2+} cation is imbedded in the benzocryptand cavity, and the acetate anion is binding to it. In the limit that the cryptand cage completely shields the Ba^{2+} cation inside the cage from the anion, relegating the anion to interact primarily with the cage walls, we would have a cage-separated ion pair. This circumstance would resemble a solvent-separated ion pair in solution, but here the benzocryptand cage serves as the cation's first solvation shell in its entirety.

On the other hand, if the acetate anion were to be able to insert itself between a pair of the three ether bridges that serve as the walls of the cage, its carboxylate end would bind directly to Ba^{2+}, forming a contact ion pair. We have not yet carried out a complete search of conformational space for the [Ba-OAc-BzCrypt]$^+$ complex, but have identified three contact ion pair minima that are likely to be among the lowest energy structures, shown in Figure 11a-c. These are shown from an end-on view down the N-Ba-N axis (N blue, Ba maroon). They all feature bidentate binding of OAc^- to Ba^{2+}, with both oxygens of the carboxylate engaged in the binding. It is unlikely that separated ion

pair structures can compete with these contact ion pairs, which are facilitated by the planar heavy-atom structure of acetate, which can slip into the crevice between any of the ether bridges. However, this is no ordinary contact ion pair, as the mode and strength of binding within the contact ion pair will be modified significantly by the presence of the molecular cage. Furthermore, the process of forming the contact ion pair requires a major deformation of the cage itself, as is evident from the structures in Figure 11, which open up on the side of the acetate anion to accommodate it.

Motivated to obtain spectroscopic signatures and structural assignments for this ion-pair cavity under gas phase conditions, we carried out both UV and IR-UV studies on [Ba-OAc-BzCrypt]$^+$. Figure 12 compares the UV photofragment spectrum of [Ba-OAc-BzCrypt]$^+$ with that of Ba^{2+}-BzCrypt studied in Section 3.1. Note that the S_0-S_1 origin of the ion-pair complex (36344 cm^{-1}) occurs just -103 cm^{-1} to the red of that for Ba^{2+}-BzCrypt, indicating that the acetate anion is not interacting strongly with the phenyl ring responsible for the UV excitation. There is also a small transition shifted an additional -23 cm^{-1} from the main electronic origin, which is likely due to a second, minor conformer of [Ba-OAc-BzCrypt]$^+$. The main electronic origin has built on it a series of low-frequency vibronic transitions involving a vibration of 18.4 cm^{-1}, for which we can see at least four members. The presence of this progression indicates that electronic excitation flexes the benzocryptand cage in the excited state relative to the ground state along this coordinate.

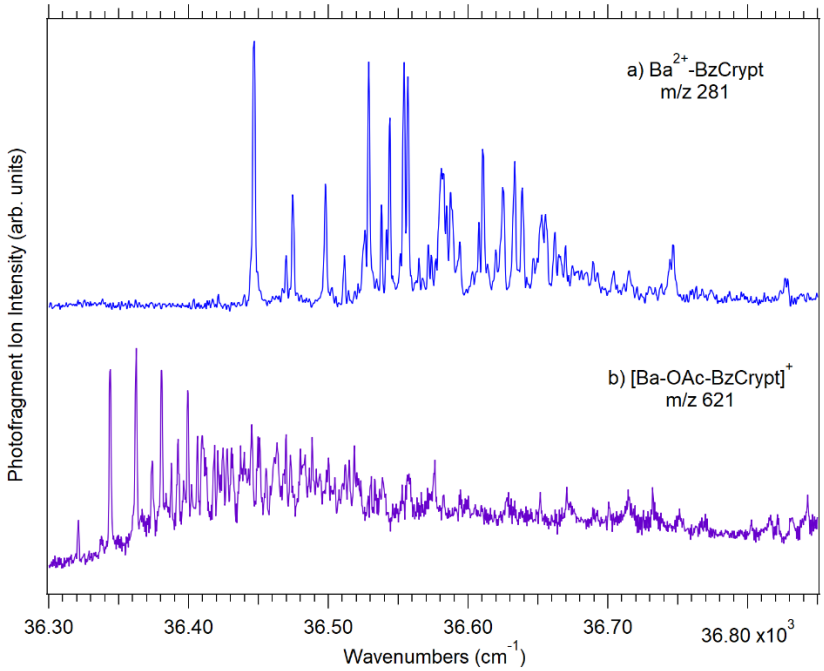

Figure 42. UV Photofragment spectrum of (a) Ba^{2+}-BzCrypt and (b) [Ba-OAc-BzCrypt]$^+$.

Figure 13 presents IR-UV gain spectra in the mid-IR region for both [Ba-OAc-BzCrypt]$^+$ and its isotope that has acetate's methyl group deuterated (OAc-d_3, $CD_3CO_2^-$). This selective isotopic substitution will assist our collaborator, Ned Sibert, in his modeling of the alkyl CH stretch spectrum, which in the presence of OAc-h_3 has methyl CH stretch transitions occurring in the same region as the benzocryptand cage. This interference is removed with OAc-d_3 substitution.

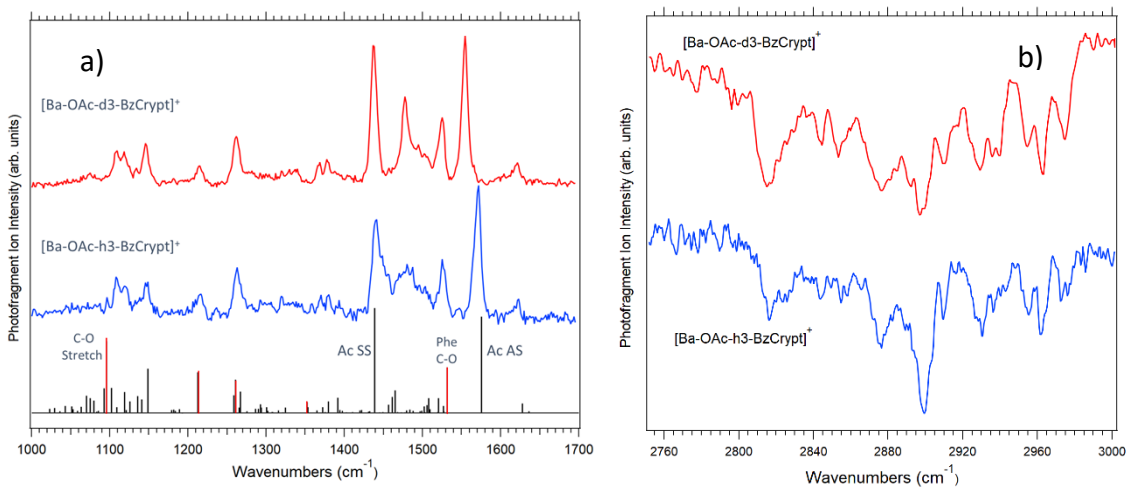

Figure 53. a) IR-UV gain spectra in the mid-IR of [Ba-OAc-BzCrypt]$^+$ and the corresponding spectrum using deuterated acetate, $CD_3CO_2^-$ (OAc-d3). The calculated spectrum for the structure in Figure 11a) is shown as a stick diagram below experiment. (b) IR-UV dip spectra in the alkyl CH stretch region.

The stick diagram below the experimental spectra is the calculated vibrational frequencies and IR intensities for the structure shown in Figure 11a). Notably, the two dominant IR transitions at 1572 and 1444 cm^{-1} are assigned to the antisymmetric stretch (AS) and symmetric stretch (SS) of the carboxylate group, CO_2^-, respectively. In a recent study by Habka *et al.*,[30] they assign an analogous pair of transitions at 1394 and 1570 cm^{-1} in the uncaged K$^+$-phenylacetate complex to the SS and AS fundamentals, respectively. Thus, while the AS fundamental is hardly changed from that in the uncaged +1/-1 ion pair K$^+$-OAc^{-1}, the SS fundamental of our +2/-1 ion pair caged complex is shifted to higher frequency by 50 cm^{-1}.

3.4.2. Using the Ion Pair to produce Ba$^+$-BzCrypt

In the course of our studies on [Ba-OAc-h3/d3-BzCrypt]$^+$, we recorded UV photofragment mass spectra with the UV laser fixed on the S_0-S_1 origins of these complexes. The mass spectrum of the OAc-d_3 complex is shown in Figure 14, with the parent mass just off-scale at 624.2 amu. The mass spectrum of both isotopologues show a common mass peak at m/z = 562 amu, which is the mass of the main Ba isotope of Ba$^+$-BzCrypt complex. In addition, there are prominent peaks at 196.4/199.4 amu due to [Ba-OAc-h3/d3]$^+$ and at 310.5/312.0 due to [Ba-OAc-BzCrypt]$^{2+}$. The peak at mass 562 is particularly interesting, as it is due to the Ba^{+1} cation trapped in the BzCrypt molecular cage. This is precisely the singly charged ion we hoped to make from the Ba^{2+}-BzCrypt complex by ion-ion reactions in the mass spectrometer,

$$Ba^{2+}\text{-BzCrypt} + X^- \rightarrow \mathbf{Ba^+\text{-}BzCrypt} + X. \qquad (1)$$

Here, we make this ion in what is formally a two-step process from the ion-pair complex, [Ba-OAc-BzCrypt]$^+$, involving electron transfer from the acetate anion to Ba^{2+}, followed by loss of the neutral acetyloxy radical, CH_3-CO_2 (•OAc),

$$[Ba^{2+}\text{-}OAc^{1-}\text{-}BzCrypt] + h\nu_{UV} \rightarrow [Ba^+\text{-BzCrypt}]\cdots OAc \rightarrow \mathbf{Ba^+\text{-}BzCrypt} + \bullet OAc. \qquad (2)$$

The other mass channels involve photodetachment of an electron from the acetate anion to form the [Ba-OAc-BzCrypt]$^{2+}$ complex with exactly half the m/z ratio since 'z' increases from +1 to +2.

Finally, the mass peak at 196.4/199.4 is due to the bare ion pair complex $[Ba\text{-}OAc]^+$, presumably by extraction of the ion pair from the benzocryptand cage.

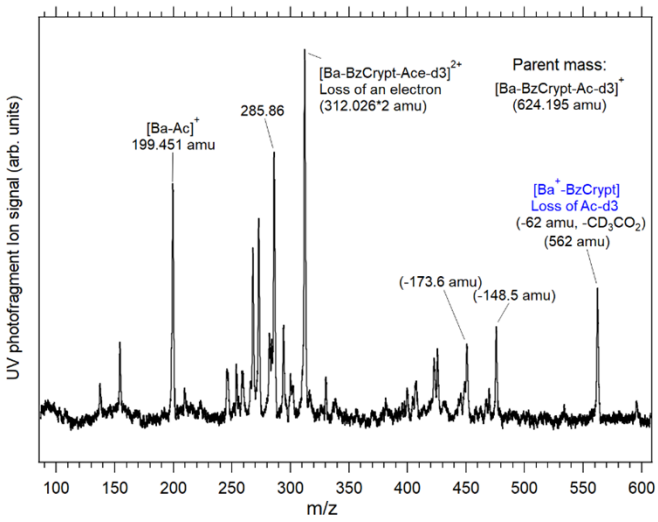

Figure 14. UV photofragment mass spectrum of $[Ba\text{-}OAc\text{-}d3\text{-}BzCrypt]^+$ with UV at 36,343 cm^{-1}.

4. CONCLUSIONS

The results described in Section 3.3 were obtained over the last few months of the LDRD grant cycle, but they are among the most important to come from our efforts, as they suggest a new strategy for making the M^+-BzCrypt complexes (M^+=Ca, Ba) that were our ultimate target for exploration in the application space of ion-trap quantum computing. We believe that ion-pair/cryptand cage complexes such as [Ba^{2+}-OAc^{1-}-BzCrypt] could be an effective starting point for formation of the desired Ca^+/Ba^+-BzCrypt complexes whose spectroscopy we sought to pursue with our methods.

As summarized in the introduction, the singly charged alkaline earth cations Ca^+ and Ba^+ are the current ions of choice for ITQC, with electronic transitions that occur at convenient wavelengths for laser cooling and qubit state preparation.[31]

We hope to be able to study this spectroscopy via follow-on funding in the future to test our original hypothesis in greater depth. One of the reasons we are enthusiastic about such studies is that we have observed that several different excitation methods all enhance formation of Ba^+-BzCrypt from [Ba-OAc-BaCrypt]$^+$, including UV excitation (Figure 14), IR excitation, and collisional excitation. Indeed, it seems plausible that we could form the [Ba-OAc-BzCrypt]$^+$ parent ion in large concentrations via electrospray ionization, mass isolate this ion-pair/cage complex, and then use near-resonant radio-frequency excitation to energize [Ba-OAc-BzCrypt]$^+$ through collisions with buffer gas until it undergoes fragmentation to form Ba^+-BzCrypt.

Beyond further exploration of these reactions in [Ba-OAc-BzCrypt]$^+$, there are other directions to explore via follow-on funding. First, other anions than acetate are likely to also engage in the analogous process of electron transfer and loss of the neutral form of the anion. A broader exploration of this chemistry would help us optimize this process from the ion-pair/cryptand complex to the point that sufficient Ba^+-BzCrypt complex can be formed for spectroscopic interrogation.

Second, we also have yet to explore analogous pathways to Ca^+-BzCrypt, but it seems likely that such pathways also exist. We are struck by the generality of this strategy, forming an ion pair-molecular cavity complex composed of a cation in its natural charge state inside a molecular cavity, but also bound to a counter-ion. Collisional or laser excitation can then be used to induce electron transfer and loss of the neutral form of the anion to form M^+-BzCrypt.

Finally, beyond ITQC applications, the possibility of trapping metal ions in unusual charge states inside cryptand cages is also worth pursuing in the context of catalysis or CO_2 capture and chemical processing.

REFERENCES

1. Brown, K. R.; Kim, J.; Monroe, C., Co-designing a scalable quantum computer with trapped atomic ions. *npj Quantum Inform.* **2016,** *2*.
2. Werth, G.; Gheorghe, V. N.; G, M. F., Quantum Computing with Trapped Charged Particles. In *Charged Particle Traps II*, Springer Series on Atomic, Optical and Plasma Physics: 2009; pp 207-256.
3. Calvin, A. T.; Brown, K. R., Spectroscopy of Molecular Ions in Coulomb Crystals. *J. Phys. Chem. Lett.* **2018,** *9* (19), 5797-5804.
4. Calvin, A. T.; Janardan, S.; Condoluci, J.; Rugango, R.; Pretzsch, E.; Shu, G.; Brown, K. R., Rovibronic Spectroscopy of Sympathetically Cooled (CaH+)-Ca-40. *J. Phys. Chem. A* **2018,** *122* (12), 3177-3181.
5. Hudson, E. R.; Campbell, W. C., Dipolar quantum logic for freely rotating trapped molecular ions. *Phys. Rev. A* **2018,** *98* (4).
6. Staanum, P. F.; Hojbjerre, K.; Skyt, P. S.; Hansen, A. K.; Drewsen, M., Rotational laser cooling of vibrationally and translationally cold molecular ions. *Nature Physics* **2010,** *6* (4), 271-274.
7. Wolf, F.; Wan, Y.; Heip, J. C.; Gebert, F.; Shi, C. Y.; Schmidt, P. O., Non-destructive state detection for quantum logic spectroscopy of molecular ions. *Nature* **2016,** *530* (7591), 457-+.
8. Allen, C. D.; Rempe, S. L. B.; Zwier, T. S.; Ren, P. Y., Trapping Ca+ inside a molecular cavity: computational study of the potential energy surfaces for Ca+- n cycloparaphenylene, n=5-12. *Phys. Chem. Chem. Phys.* **2022,** *24* (17), 10085-10094.
9. Garcia, E. A.; Gomis, D. B., Extraction-spectrofluorimetric determination of thallium using cryptand ethers. *Anal. Lett.* **2002,** *35* (14), 2337-2346.
10. Jin, G. X.; Bailey, M. D.; Allen, M. J., Unique Eu-II Coordination Environments with a Janus Cryptand. *Inorg. Chem.* **2016,** *55* (17), 9085-9090.
11. Pfrunder, M. C.; Marshall, D. L.; Poad, B. L. J.; Stovell, E. G.; Loomans, B. I.; Blinco, J. P.; Blanksby, S. J.; McMurtrie, J. C.; Mullen, K. M., Exploring the Gas-Phase Formation and Chemical Reactivity of Highly Reduced M8L6 Coordination Cages. *Angewandte Chemie-International Edition* **2022,** *61* (45).
12. Wordsworth, J.; Benedetti, T. M.; Somerville, S. V.; Schuhmann, W.; Tilley, R. D.; Gooding, J. J., The Influence of Nanoconfinement on Electrocatalysis. *Angewandte Chemie-International Edition* **2022,** *61* (28).
13. Zhou, K.; Xu, Z. P., Nanoconfinement-Enforced Ion Correlation and Nanofluidic Ion Machinery. *Nano Lett.* **2020,** *20* (11), 8392-8398.
14. Burke, N. L.; DeBlase, A. F.; Redwine, J. G.; Hopkins, J. R.; McLuckey, S. A.; Zwier, T. S., Gas-Phase Folding of a Prototypical Protonated Pentapeptide: Spectroscopic Evidence for Formation of a Charge-Stabilized beta-Hairpin. *J. Am. Chem. Soc.* **2016,** *138* (8), 2849-2857.
15. Zhang, C.; Chen, H. W.; Guymon, A. J.; Wu, G. X.; Cooks, R. G.; Ouyang, Z., Instrumentation and methods for ion and reaction monitoring using a non-scanning rectilinear ion trap. *Int. J. Mass spectrom.* **2006,** *255*, 1-10.
16. Paizs, B.; Suhai, S., Comparative study of BSSE correction methods at DFT and MP2 levels of theory. *J. Comput. Chem.* **1998,** *19* (6), 575-584.
17. Walker, B.; Liu, C. W.; Wait, E.; Ren, P. Y., Automation of AMOEBA polarizable force field for small molecules: Poltype 2. *J. Comput. Chem.* **2022,** *43* (23), 1530-1542.
18. Kim, S.; Chen, J.; Cheng, T.; Gindulyte, A.; He, J.; He, S.; Li, Q.; Shoemaker, B. A.; Thiessen, P. A.; Yu, B., et. al., PubChem 2023 update. *Nucleic Acids Res.* **2022,** *51* (D1), D1373-D1380.

19. Romo, T. D.; Leioatts, N.; Grossfield, A., Lightweight Object Oriented Structure Analysis: Tools for Building Tools to Analyze Molecular Dynamics Simulations. *J. Comput. Chem.* **2014,** *35* (32), 2305-2318.
20. Frisch, M. J.; Trucks, G. W.; Schlegel, H. B.; Scuseria, G. E.; Robb, M. A.; Cheeseman, J. R.; Scalmani, G.; Barone, V.; Petersson, G. A.; Nakatsuji, H., et. al. *Gaussian 16 Rev. C.01*, Wallingford, CT, 2016.
21. Chaudhari, M. I.; Vanegas, J. M.; Pratt, L. R.; Muralidharan, A.; Rempe, S. B., Hydration Mimicry by Membrane Ion Channels. In *Ann. Rev. Phys. Chem.*, Johnson, M. A.; Martinez, T. J., Eds. 2020; Vol. 71, pp 461-484.
22. Rempe, S. B.; Asthagiri, D.; Pratt, L. R., Inner shell definition and absolute hydration free energy of K+(aq) on the basis of quasi-chemical theory and ab initio molecular dynamics. *Phys. Chem. Chem. Phys.* **2004,** *6* (8), 1966-1969.
23. Jing, Z. F.; Rackers, J. A.; Pratt, L. R.; Liu, C. W.; Rempe, S. B.; Ren, P. Y., Thermodynamics of ion binding and occupancy in potassium channels. *Chem. Sci.* **2021,** *12*, 8920.
24. Chaudhari, M. I.; Soniat, M. L.; Rempe, S. B., Octa-Coordination and the Aqueous Ba2+ Ion. *J. Phys. Chem. B* **2015,** *119* (28), 8746-8753.
25. Foley, C. D.; Allen, C. D.; Au, K.; Lee, C.; Rempe, S. B.; Ren, P.; Sibert, E. L., III; Zwier, T. S., Molecular Cage Reports on Its Contents: Spectroscopic Signatures of Cryo-Cooled K+- and Ba2+-Benzocryptand Complexes. *The Journal of Physical Chemistry A* **2023,** *127* (30), 6227-6240.
26. Tuttle, W. D.; Gardner, A. M.; Andrejeva, A.; Kemp, D. J.; Wakefield, J. C. A.; Wright, T. G., Consistent assignment of the vibrations of symmetric and asymmetric ortho-disubstituted benzenes. *I. Mol. Spectrosc.* **2018,** *344*, 46-60.
27. Lee, Chin; Allen, Cole D.; Au, Kendrew; Foley, Casey D.; Rempe, Susan B.; Ren, Pengyu; Sibert III, Edwin L.; Zwier, Timothy S., Periodic Trends in Cation Binding inside Cryptand Molecular Cages. **in preparation**.
28. Yi, J. T.; Ribblett, J. W.; Pratt, D. W., Rotationally Resolved Electronic Spectra of 1,2-Dimethoxybenzene and the 1,2-Dimethoxybenzene−Water Complex. *The Journal of Physical Chemistry A* **2005,** *109* (42), 9456-9464.
29. Lee, Chin; Au, Kendrew; Allen, Cole D.; Rempe, Susan B.; Ren, Pengyu; Sibert III, Edwin L.; Zwier, Timothy S., Parting the Walls of a Molecular Cage to form an Ion-Pair Complex: Spectroscopy and Photochemistry of [Ba^{2+}-$Acetate^{-}$-Benzocryptand] Complexes. **in preparation**.
30. Habka, S.; Very, T.; Donon, J.; Vaquero-Vara, V.; Tardivel, B.; Charnay-Pouget, F.; Mons, M.; Aitken, D. J.; Brenner, V.; Gloaguen, E., Identification of ion pairs in solution by IR spectroscopy: crucial contributions of gas phase data and simulations. *Phys. Chem. Chem. Phys.* **2019,** *21* (24), 12798-12805.
31. Alsing, P.; Battle, P.; Bienfang, J. C.; Borders, T.; Brower-Thomas, T.; Carr, L. D.; Chong, F.; Dadras, S.; DeMarco, B.; Deutsch, I.; Figueroa, E.; Freedman, D.; Everitt, H.; Gauthier, D.; Johnston-Halperin, E.; Kim, J.; Kira, M.; Kumar, P.; Kwiat, P.; Lekki, J.; Loiacono, A.; Loncar, M.; Lowell, J. R.; Lukin, M.; Merzbacher, C.; Miller, A.; Monroe, C.; Pollanen, J.; Pappas, D.; Raymer, M.; Reano, R.; Rodenburg, B.; Savage, M.; Searles, T.; Ye, J., Accelerating Progress Towards Practical Quantum Advantage: The Quantum Technology Demonstration Project Roadmap. *arXiv:2210.14757v3*.

DISTRIBUTION

Email—Internal

Name	Org.	Sandia Email Address
Nils Hansen	8353	nhansen@sandia.gov
David Chandler	8353	chand@sandia.gov
Craig Taatjes	8350	cataatj@sandia.gov
Rick Muller	5220	rmuller@sandia.gov
Daniel Stick	5225	dlstick@sandia.gov
Susan M. Clark	5225	sclark@sandia.gov
Technical Library	1911	sanddocs@sandia.gov

Email—External

Name	Company Email Address	Company Name
Evan Williams	erw@berkeley.edu	UC-Berkeley
Kristin Bowman-James	kbjames@ku.edu	University of Kansas

This page left blank

Sandia National Laboratories

Sandia National Laboratories is a multimission laboratory managed and operated by National Technology & Engineering Solutions of Sandia LLC, a wholly owned subsidiary of Honeywell International Inc. for the U.S. Department of Energy's National Nuclear Security Administration under contract DE-NA0003525.